DELFT UNIVERSITY OF TECHNOLOGY

REPORT 01-10

On the Dynamics of a Single Seesaw Oscillator Under Strong Wind Conditions

H. Lumbantobing

ISSN 1389-6520

Reports of the Department of Applied Mathematical Analysis

Delft 2001

ON THE DYNAMICS OF A SINGLE SEESAW OSCILLATOR UNDER STRONG WIND CONDITIONS

H. Lumbantobing*†

Abstract

This paper is concerned with the dynamics of a one degree of freedom single seesaw structure in a steady wind flow. We assume strong wind conditions inducing nonlinear aeroelastic stiffness forces that are of the same order of magnitude as the structural stiffness forces. As model equation for the aeroelastic behaviour of the single seesaw structure we obtain a strongly nonlinear self-excited oscillator. We study the bifurcation and the stability of limit cycles for this equation using a special perturbation method. Both the case with linear structural stiffness and the case with nonlinear structural stiffness are studied. For both cases we consider a general cubic approximation to describe the aerodynamic coefficient. Conditions for the existence, the stability, and the bifurcation of limit cycles are given.

1 Introduction

We consider the dynamics of a one-degree-of-freedom single seesaw oscillator placed in a homogeneous and uniform wind flow. A schematic sketch of this oscillator is given in Figure 1. This seesaw like structure consists of two parallel rigid bars hinged around an axis. The bars hold between their right ends a cylinder, parallel to the hinge axis. On the other ends two counterweights are fixed balancing the cylinder with respect to the hinge axis. The vertical pendulum weights fixed to the bars provide for a restoring moment. If the cylinder has a non-circular cross section and is exposed to a homogeneous and uniform wind flow, self-excited so called galloping oscillations may arise [1]. Haaker and van der Burgh [2] modelled and analyzed the equation of motion of the single seesaw oscillator for low flow velocities. The wind forces then act as a perturbation on the *linear* Hamiltonian system modelling the unforced oscillations of the seesaw structure for small amplitudes. For higher flow velocities, i.e. strong wind, large aerodynamic stiffness forces appear that,

*On leave from Jurusan Matematika, FKIP, Universitas Cenderawasih - Jayapura, Indonesia.

†Department of Applied Mathematical Analysis, Faculty of Information Technology and System, Delft University of Technology, Mekelweg 4, 2628 CD Delft, The Netherlands

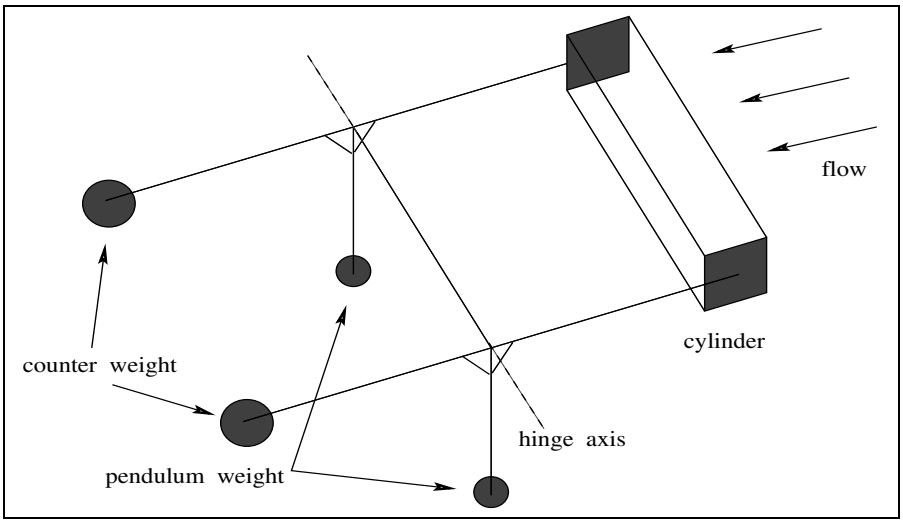

Figure 1: Schematic sketch of the structure of the single seesaw oscillator.

when included in the Hamiltonian system, give rise to a perturbed, strongly *nonlinear* Hamiltonian system. In [3] such a system was analyzed for the special case of a cylinder with rectangular cross-section. Here we consider a more general class of cross-sections, i.e. we assume the aerodynamic coefficient curve can be modelled with a cubic polynomial. Moreover, we extend the analysis to allow for nonlinear structural stiffness.
The model equation we obtain is a perturbed nonlinear Hamiltonian system. The study of limit cycles for this type of system is generally based on the study of fixed points of a certain Poincaré map. Alternatively one may study the zeroes of the associated distance function, often referred to as the Poincaré-Melnikov function. Doelman and Verhulst [4] applied this method to study the bifurcations of certain strongly nonlinear self-excited oscillators. Van Horssen and Kooij [5] considered the bifurcation of limit cycles for a particular class of quadratic systems with two centers. Iliev and Perko [6] consider the asymmetrically perturbed Duffing equation. These last authors rewrite the Poincaré-Melnikov function as a sum of integral quotients, a method we also adopt here.
This paper is organized as follows. We begin with deriving our model equation for the aeroelastic response of the single seesaw oscillator. Following that, we start the analysis by assuming the structural stiffness to be linear. We consider the existence, the stability, and the bifurcation of limit cycles for three particular choices of the aerodynamic coefficient $C_N(\alpha)$, related to the shape of the cylinder's cross-section. Next we turn to the analysis for the case with nonlinear structural stiffness. Then the unforced oscillations are modeled by a *nonlinear* Hamiltonian system. For each case we present phase portraits for a representative numerical example. We end the paper with some conclusions.

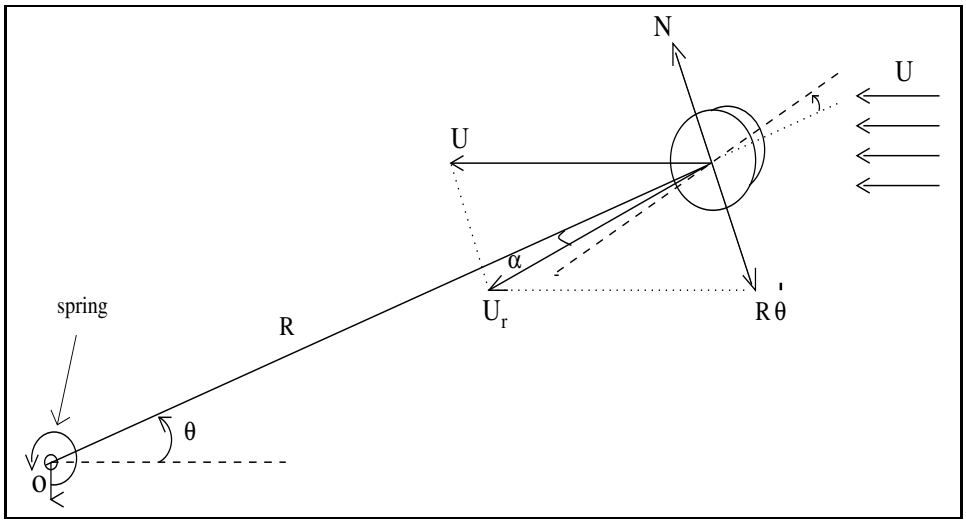

Figure 2: Quasi-steady modelling of seesaw galloping.

2 Derivation of the model equation

We summarize the result of [7] in which the equation for the aeroelastic response of the single seesaw oscillator is derived, assuming linear structural stiffness forces and low flow velocities. The wind forces are modelled using a quasi-steady theory.
The angle described by the arm holding the cylinder is indicated by θ, being positive in counter clockwise direction. The distance from the cylinder's axis to the pivot O is denoted by R, see Figure 2.
The aerodynamic moment M exerted on the structure is modelled using the transversal component N of the aerodynamic force exerted on the cylinder. To find N we use a quasi steady approach, that is, we assume N in the dynamic situation to be given by the force experienced in the equivalent static situation [7]. Then N is given by $N = \frac{1}{2}\rho l d U_r^2 C_N(\alpha)$ [1], with ρ the density of air, l the length of the cylinder, d is a typical measure for the cylinder cross-section (i.e., diameter for circular section, side-face for rectangular section). $C_N(\alpha)$ is an aerodynamic coefficient curve that depends solely on the shape of the cylinder cross-section and the orientation α towards the experienced flow U_r, see Figure 2. This curve may be obtained from static wind tunnel measurements. The orientation, or angle of attack α, is approximately given by $\alpha = \theta - \frac{R\dot{\theta}}{U}$. Using the aerodynamic coefficient curve $C_N(\alpha)$, the aerodynamic moment is now approximately given by

$$M(\alpha) = \frac{1}{2}\rho d l R U^2 C_N(\alpha). \tag{2.1}$$

As a model equation we get

$$I\ddot{\theta} + c_\theta \dot{\theta} + F(\theta) = \frac{1}{2}\rho d l R U^2 C_N(\alpha), \tag{2.2}$$

with

$$F(\theta) \;=\; k\theta + \tilde{p}_2\theta^2 + \tilde{p}_3\theta^3. \tag{2.3}$$

Here I denotes the structural moment of inertia, $c_\theta > 0$ is the linear viscous damping coefficient, and $F(\theta)$ denotes the restoring structural stiffness force where $\tilde{p}_3 < 0$ is assumed. Scaling time with $\tau = \omega_\theta t$ where $\omega_\theta^2 = \frac{k}{I}$, and introducing $\epsilon = \frac{\rho d l R^3}{2I}$, $u = \frac{U}{\omega_\theta R}$, $2\xi\epsilon = \frac{c_\theta}{\omega_\theta I}$, and after simplifying we obtain an equation of motion as follows

$$\ddot{\theta} + \theta + p_2\theta^2 + p_3\theta^3 \;=\; \epsilon\left(-2\,\xi\,\dot{\theta} + u^2 C_N(\alpha)\right). \tag{2.4}$$

Here $0 < \epsilon \ll 1$ is a small constant which may be interpreted as a measure for the ratio of displaced air mass to cylinder mass. Note that u is the non dimensional wind velocity. Throughout this paper we assume $C_N(\alpha)$ to be cubic, i.e.

$$C_N(\alpha) \;=\; c_1\alpha + c_2\alpha^2 + c_3\alpha^3,$$

with $c_1 < 0$ and $c_3 \geq 0$.
Substituting for α and $C_N(\alpha)$, we now write (2.4) as follows

$$\begin{aligned}\ddot{\theta} + (1 - c_1u^2\epsilon)\theta + (p_2 - c_2u^2\epsilon)\theta^2 + (p_3 - \epsilon u^2 c_3)\theta^3 = \epsilon u\Bigg(-\left(\frac{2\xi}{u} + c_1\right)\dot{\theta} \\ + \frac{c_2}{u}\dot{\theta}^2 - 2c_2\theta\dot{\theta}^2 - 3c_3\theta^2\dot{\theta} + \frac{3c_3}{u}\theta\dot{\theta} - \frac{c_3}{u^2}\dot{\theta}^3\Bigg).\end{aligned} \tag{2.5}$$

Assuming a strong wind velocity u, i.e. $\epsilon u^2 = \mathcal{O}(1)$, we may introduce a new $\mathcal{O}(1)$ parameter $\kappa = \epsilon u^2$ and a new small parameter $\tilde{\epsilon} = \epsilon u = \sqrt{\epsilon\kappa}$ to equation (2.5) to obtain

$$\begin{aligned}\ddot{\theta} + (1 - c_1\kappa)\,\theta + (p_2 - c_2\kappa)\,\theta^2 + (p_3 - c_3\kappa)\,\theta^3 \;&=\; \tilde{\epsilon}\left(-c_1\dot{\theta} - 2\,c_2\,\theta\,\dot{\theta} - 3\,c_3\theta^2\dot{\theta}\right) \\ &+\; \mathcal{O}(\tilde{\epsilon}^2).\end{aligned} \tag{2.6}$$

We rescale $t \to \frac{s}{\sqrt{1-c_1\kappa}}$ then the system (2.6) becomes

$$\begin{aligned}(1 - c_1\kappa)\,\ddot{\theta} + (1 - c_1\kappa)\,\theta + (p_2 - c_2\kappa)\,\theta^2 + (p_3 - c_3)\kappa\,\theta^3 = \\ \tilde{\epsilon}\left(-c_1\sqrt{1 - c_1\kappa}\,\dot{\theta} - 2\,c_2\sqrt{1 - c_1\kappa}\,\theta\,\dot{\theta} - 3\,c_3\sqrt{1 - c_1\kappa}\,\theta^2\dot{\theta}\right) + \mathcal{O}(\tilde{\epsilon}^2).\end{aligned} \tag{2.7}$$

Dividing both sides by $1 - c_1\kappa > 0$ we get

$$\ddot{\theta} + \theta + \alpha_{20}\theta^2 + \alpha_{30}\theta^3 = \tilde{\epsilon}\left(\alpha_{01}\,\dot{\theta} + \alpha_{11}\theta\,\dot{\theta} + \alpha_{21}\theta^2\dot{\theta}\right) + \mathcal{O}(\tilde{\epsilon}^2), \tag{2.8}$$

with

$\alpha_{01} = -\frac{c_1}{\sqrt{1-c_1\kappa}} > 0$, $\qquad \alpha_{21} = -3\,\frac{c_3}{\sqrt{1-c_1\kappa}} \leq 0$,
$\alpha_{11} = -2\,\frac{c_2}{\sqrt{1-c_1\kappa}}$, $\qquad \alpha_{20} = \frac{p_2 - c_2\kappa}{1-c_1\kappa}$.
$\alpha_{30} = \frac{p_3 - c_3\kappa}{1-c_1\kappa} \leq 0$,

This is a perturbed Hamiltonian system with Hamiltonian

$$H(\theta, \dot{\theta}) = \frac{1}{2}\dot{\theta}^2 + \frac{1}{2}\theta^2 + \frac{1}{3}\,\alpha_{20}\theta^3 + \frac{1}{4}\,\alpha_{30}\theta^4. \tag{2.9}$$

3 Analysis of the model equation for linear structural stiffness

In this section we consider the existence, the bifurcation, and the stability of limit cycles for the linear seesaw oscillator, i.e. equation (2.4) with $p_2 = p_3 = 0$. We consider three special choices of the parameters c_1, c_2, and c_3.

3.1 Cubic symmetrical $C_N(\alpha)$ case

In this subsection we assume the cylinder's cross section to be symmetrical and the symmetry axis to coincide with the arm holding the cylinder, implying $c_2 = 0$. We can write the system (2.8) as

$$\ddot{\theta} + \theta + \tilde{\alpha}_{30}\theta^3 = \tilde{\epsilon}\,\left(\alpha_{01}\,\dot{\theta} + \alpha_{21}\theta^2\dot{\theta}\right) + \mathcal{O}(\tilde{\epsilon}^2), \tag{3.1}$$

where $\tilde{\alpha}_{30} = -\frac{c_3\kappa}{1-c_1\kappa} < 0$.
We rescale $\theta \to c\,\bar{\theta}$, then, after neglecting the "bar" and choosing $c = \frac{1}{\sqrt{-\tilde{\alpha}_{30}}}$ we get

$$\ddot{\theta} + \theta - \theta^3 = \tilde{\epsilon}\,\left(\alpha_{01}\,\dot{\theta} - \frac{\alpha_{21}}{\tilde{\alpha}_{30}}\theta^2\dot{\theta}\right) + \mathcal{O}(\tilde{\epsilon}^2). \tag{3.2}$$

This is a perturbed Hamiltonian system with Hamiltonian

$$H(\theta,\dot{\theta}) = \frac{1}{2}\dot{\theta}^2 + \frac{1}{2}\theta^2 - \frac{1}{4}\theta^4. \tag{3.3}$$

Letting $\theta = \theta_1$ and $\dot{\theta} = \theta_2$ we get

$$\begin{cases} \dot{\theta_1} = \theta_2, \\ \dot{\theta_2} = -\theta_1 + \theta_1^3 + \tilde{\epsilon}\left(\alpha_{01}\theta_2 - \frac{\alpha_{21}}{\tilde{\alpha}_{30}}\,\theta_1^2\theta_2\right) + \mathcal{O}(\tilde{\epsilon}^2). \end{cases} \tag{3.4}$$

The critical points of the unperturbed system are $(0,0)$ and $(\pm 1, 0)$. Note that $(0,0)$ is a center point and $(\pm 1, 0)$ are saddle points. We observe that for each h with $0 < h < h_{max}$, the equation $H(\theta,\dot{\theta}) = h$ represents a periodic orbit γ_h surrounding the center point $(0,0)$. The periodic orbits are bounded by two heteroclinic orbits, connecting the two saddle points, obtained from $H(\theta,\dot{\theta}) = h_{max} = \frac{1}{4}$. In order to determine the number of limit cycles of (3.4) we use Pontryagin's method for perturbed Hamiltonian systems, described, e.g. in theorem 78 of [8]. This (first order) perturbation theorem shows that precisely one structurally stable limit cycle is bifurcated out of the periodic orbit $\gamma(h_0)$ of the unperturbed system (3.4) if the Poincaré-Melnikov function $I(h)$, given by,

$$I(h) = \oint_{\gamma_h} \left(\alpha_{01}\dot{\theta} - \frac{\alpha_{21}}{\tilde{\alpha}_{30}}\,\theta^2\dot{\theta}\right)\,d\theta, \tag{3.5}$$

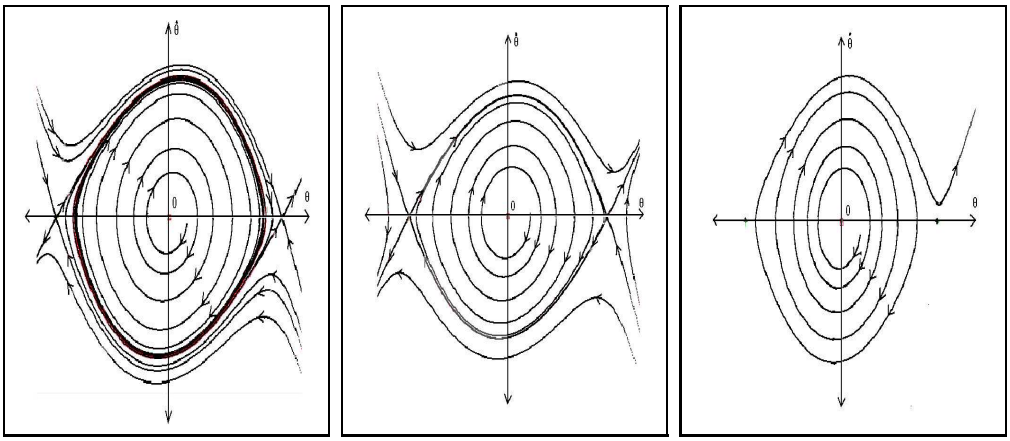

(a) $\kappa = 0.3$ (b) $\kappa = 0.5$ (c) $\kappa = 0.7$

Figure 3: Phase portraits of cubic symmetrical $C_N(\alpha)$ case for $c_1 = -3$, $c_3 = 1$, $\tilde{\epsilon} = 0.07$.

has a simple zero at $h = h_0$, that is, $I(h_0) = 0$ and $\frac{dI}{dh}(h_0) < 0$. We write the Poincaré-Melnikov function using an integral quotient as follows

$$\begin{aligned} I(h) &= 4\left(\alpha_{01} I_0(h) - \frac{\alpha_{21}}{\tilde{\alpha}_{30}} I_2(h)\right), \\ &= 4\alpha_{01} I_0(h)\left(1 - \frac{\alpha_{21}}{\alpha_{01}\tilde{\alpha}_{30}} \frac{I_2(h)}{I_0(h)}\right), \\ &= 4\alpha_{01} I_0(h)\left(1 - \frac{\alpha_{21}}{\alpha_{01}\tilde{\alpha}_{30}} Q_{20}(h)\right), \end{aligned}$$

where $I_0(h) = \int_0^{\theta(h)} \dot{\theta} d\theta$, $I_2(h) = \int_0^{\theta(h)} \theta^2 \dot{\theta} d\theta$, $\dot{\theta} = \sqrt{G(\theta)}$ with $G(\theta) = 2h - \theta^2 + \frac{1}{2}\theta^4$, $Q_{31}(h) = \frac{I_2(h)}{I_0(h)}$, and the upper boundary of the integrals, $\theta(h)$, is the smallest positive zero of $G(\theta)$.

In appendix 1, it is shown that $Q_{20}(h)$ is a strictly increasing function in h. The function $I(h)$ has at most one zero depending on the sign of $\frac{\alpha_{21}}{\alpha_{01}\tilde{\alpha}_{30}}$. This means that there is at most one limit cycle [9]. We now consider the existence of this limit cycle. Consider that $Q_{20}(0) = 0$, $Q_{20}(h_{max}) = \frac{1}{5}$, and $I(h) = 0$ if and only if $Q_{20}(h) = \frac{\alpha_{01}\tilde{\alpha}_{30}}{\alpha_{21}} = \frac{c_1\kappa}{3c_1\kappa - 3}$. Then we conclude that the limit cycle exists if and only if $0 < \frac{c_1\kappa}{3c_1\kappa-3} < \frac{1}{5}$, i.e. $\kappa < -\frac{3}{2c_1}$ and a heteroclinic bifurcation occurs for $\kappa = -\frac{3}{2c_1}$. The limit cycle is always stable as $\frac{dI}{dh}(h) < 0$. Numerical results for some special values of the parameters are shown in Figure 3. For $\kappa = 0.3$ we find a stable limit cycle. For $\kappa = 0.5$ the limit cycle disappears in a heteroclinic bifurcation. For $\kappa = 0.7$ the system is globally unstable and any initial disturbance leads to an unbounded solution.

3.2 Quadratic $C_N(\alpha)$ case

In this subsection we assume the cylinder's cross section to be asymmetrical such that a quadratic $C_N(\alpha)$ may be assumed. Assuming $c_1 < 0$ and $c_2 \neq 0$, the system (2.8) becomes

$$\ddot{\theta} + \theta + \tilde{\alpha}_{20}\theta^2 = \tilde{\epsilon}(\alpha_{01}\dot{\theta} + \alpha_{11}\theta\,\dot{\theta}) + \mathcal{O}(\tilde{\epsilon}^2), \tag{3.6}$$

where $\tilde{\alpha}_{20} = -\frac{c_2\kappa}{1-c_1\kappa}$.
We rescale $\theta \to c\,\bar{\theta}$, then, after neglecting the "bar" and choosing $c = \frac{-1}{\tilde{\alpha}_{20}}$ we get

$$\ddot{\theta} + \theta - \theta^2 = \tilde{\epsilon}\,\left(\alpha_{01}\,\dot{\theta} - \frac{\alpha_{11}}{\tilde{\alpha}_{20}}\theta\dot{\theta}\right) + \mathcal{O}(\tilde{\epsilon}^2). \tag{3.7}$$

This is a perturbed Hamiltonian system with Hamiltonian

$$H(\theta,\dot{\theta}) = \frac{1}{2}\dot{\theta}^2 + \frac{1}{2}\theta^2 - \frac{1}{3}\theta^3. \tag{3.8}$$

Letting $\theta = \theta_1$ and $\dot{\theta} = \theta_2$ we get

$$\begin{cases} \dot{\theta_1} = \theta_2, \\ \dot{\theta_2} = -\theta_1 + \theta_1^2 + \tilde{\epsilon}\left(\alpha_{01}\theta_2 - \frac{\alpha_{11}}{\tilde{\alpha}_{20}}\,\theta_1\theta_2\right) + \mathcal{O}(\tilde{\epsilon}^2). \end{cases} \tag{3.9}$$

The critical points of the unperturbed system are $(0,0)$ and $(1,0)$. Note that $(0,0)$ is a center point and $(1,0)$ is a saddle point. We observe that for each h with $0 < h < h_{max}$, the equation $H(\theta,\dot{\theta}) = h$ represents a periodic orbit γ_h surrounding the center point $(0,0)$. The periodic orbits are bounded by a homoclinic orbit, connecting the saddle point to itself, obtained from $H(\theta,\dot{\theta}) = h_{max} = \frac{1}{6}$. Again, we use Pontryagin's method to determine the number and the stability of limit cycles for (3.9). The Poincaré-Melnikov function is given by

$$I(h) = \oint_{\gamma_h}\left(\alpha_{01}\dot{\theta} - \frac{\alpha_{11}}{\tilde{\alpha}_{20}}\,\theta\dot{\theta}\right)\,d\theta. \tag{3.10}$$

We write the Poincaré-Melnikov function using an integral quotient as follows

$$I(h) = 2\alpha_{01}I_0(h)\left(1 - \frac{\alpha_{11}}{\alpha_{01}\tilde{\alpha}_{20}}Q_{10}(h)\right), \tag{3.11}$$

where $I_0(h) = \int_{\theta_0(h)}^{\theta_1(h)}\dot{\theta}d\theta$, $I_1(h) = \int_{\theta_0(h)}^{\theta_1(h)}\theta\dot{\theta}d\theta$, $\dot{\theta} = \sqrt{G(\theta)}$ with $G(\theta) = 2h - \theta^2 + \frac{2}{3}\theta^3$, $Q_{21}(h) = \frac{I_1(h)}{I_0(h)}$, and the boundaries of the integrals, $\theta_0(h)$ and $\theta_1(h)$, are the negative root and the smallest positive root of $G(\theta)$, respectively.
In appendix 2, it is shown that $Q_{10}(h)$ is a strictly increasing function in h.
The function $I(h)$ has at most one zero depending on the sign of $\frac{\alpha_{11}}{\alpha_{01}\tilde{\alpha}_{20}}$. We conclude that the system has at most one limit cycle. We now consider the existence of this limit cycle. Consider that $Q_{10}(0) = 0$, $Q_{10}(h_{max}) = \frac{1}{7}$, and $I(h) = 0$ if and only if $Q_{10}(h) = \frac{\alpha_{01}\tilde{\alpha}_{20}}{\alpha_{11}} = \frac{c_1\kappa}{2c_1\kappa-2}$. Then we conclude that the limit cycle exists if and only if $0 < \frac{c_1\kappa}{2c_2\kappa-2} < \frac{1}{7}$, i.e.

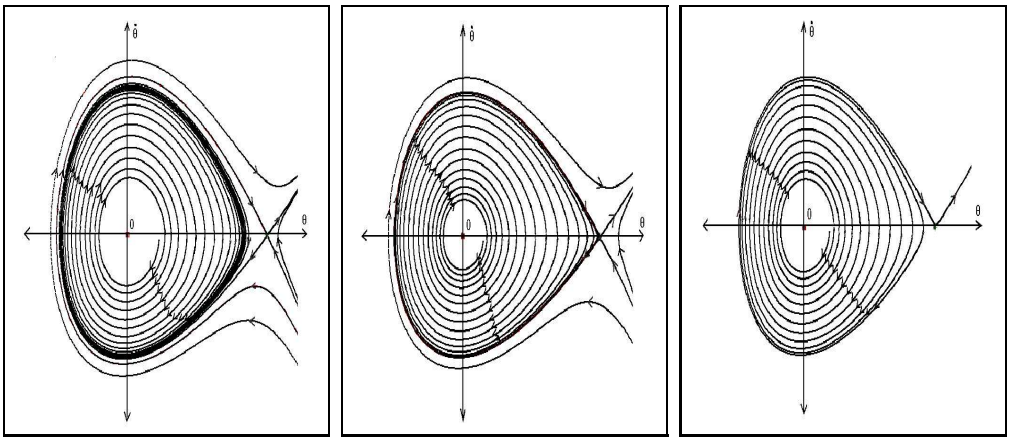

(a) $\kappa = 0.1$ (b) $\kappa = 0.133$ (c) $\kappa = 0.14$

Figure 4: Phase portraits of quadratic $C_N(\alpha)$ case for $c_1 = -3$, $c_2 = -4$, and $\tilde{\epsilon} = 0.02$.

$\kappa < -\frac{2}{5c_1}$ and a homoclinic bifurcation occurs for $\kappa = -\frac{2}{5c_1}$. The limit cycle is always stable as $\frac{dI}{dh}(h) < 0$. Numerical results for some special values of the parameters are given in Figure 4. For $\kappa = 0.1$ there is a stable limit cycle. For $\kappa = 0.132$ the limit cycle disappears in a homoclinic bifurcation. For $\kappa = 0.14$ the system is globally unstable and any initial disturbance leads to an unbounded solution.

3.3 General cubic $C_N(\alpha)$ case

In this subsection we consider the general cubic approximation for $C_N(\alpha)$ with $c_1 < 0$ and $c_3 > 0$. We rescale $\theta \to c\,\bar{\theta}$, then, after neglecting the "bar" and choosing $c = \frac{-1}{\tilde{\alpha}_{20}}$ the system (2.8) becomes

$$\ddot{\theta} + \theta - \theta^2 + \eta\,\theta^3 = \tilde{\epsilon}\,\alpha_{01}\,\left(\dot{\theta} + \beta\,\theta\,\dot{\theta} + \gamma\,\theta^2\dot{\theta}\right) + \mathcal{O}(\tilde{\epsilon}^2), \tag{3.12}$$

where $\eta = \frac{\tilde{\alpha}_{30}}{\tilde{\alpha}_{20}^2} < 0$, $\beta = \frac{-\alpha_{11}}{\alpha_{01}\tilde{\alpha}_{20}} < 0$, and $\gamma = \frac{\alpha_{21}}{\alpha_{01}\tilde{\alpha}_{20}^2} < 0$.
This is a perturbed Hamiltonian system with Hamiltonian

$$H(\theta, \dot{\theta}, \eta) = \frac{1}{2}\dot{\theta}^2 + \frac{1}{2}\theta^2 - \frac{1}{3}\theta^3 + \frac{\eta}{4}\theta^4. \tag{3.13}$$

Letting $\theta = \theta_1$ and $\dot{\theta} = \theta_2$ the system (3.12) becomes

$$\begin{cases} \dot{\theta_1} = \theta_2, \\ \dot{\theta_2} = -\theta_1 + \theta_1^2 - \eta\,\theta_1^3 + \tilde{\epsilon}\,\alpha_{01}\,\left(\theta_2 + \beta\,\theta_1\,\theta_2 + \gamma\,{\theta_1}^2\theta_2\right) + \mathcal{O}(\tilde{\epsilon}^2). \end{cases} \tag{3.14}$$

The critical points of the unperturbed system are $(0,0)$ and $(\frac{1\pm\sqrt{1-4\,\eta}}{2\,\eta}, 0)$. Note that $(0,0)$ is a center point and $(\frac{1\pm\sqrt{1-4\,\eta}}{2\,\eta}, 0)$ are saddle points. We observe that for each h with

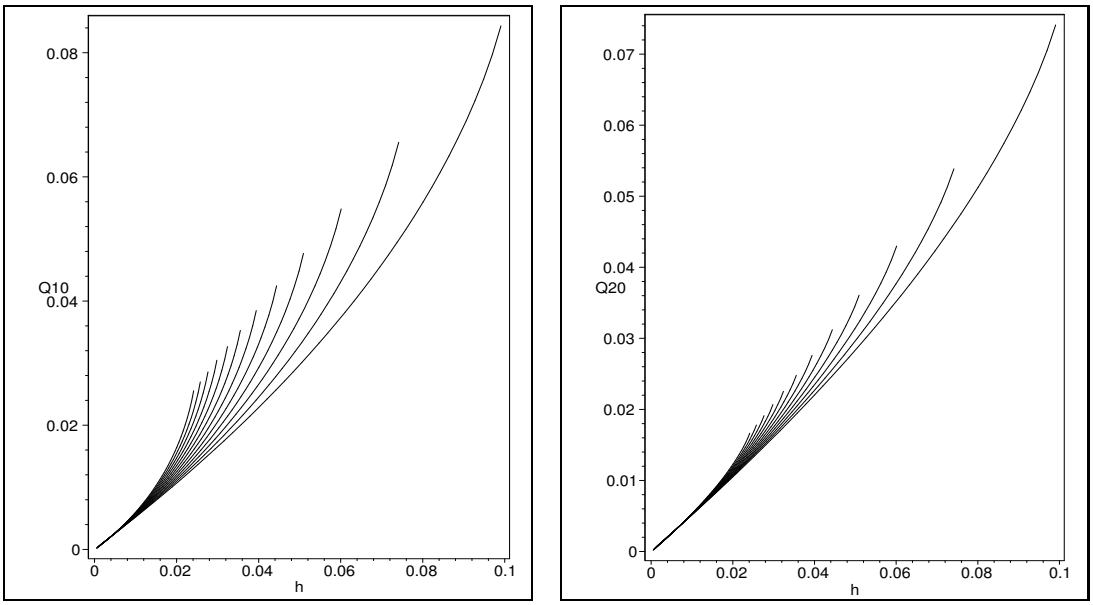

(a) Function $Q_{10}(h)$ (b) Function $Q_{20}(h)$

Figure 5: Numerical results of integral quotients $Q_{10}(h,\eta)$ and $Q_{20}(h,\eta)$ for several values of η.

$0 < h < h_{max}$, the equation $H(\theta,\dot{\theta}) = h$ represents a periodic orbit γ_h, surrounding the center point $(0,0)$. The periodic orbits are bounded by a homoclinic orbit, connecting the saddle point closest to the center point to itself. The homoclinic orbit is obtained from $H(\theta,\dot{\theta},\eta) = h_{max} = \frac{1}{96}\,\frac{\left(1+\sqrt{1-4\,\eta}\right)^2\left(6\,\eta-1-\sqrt{1-4\,\eta}\right)}{\eta^3}$. The Poincaré-Melnikov function is given by

$$I(h,\eta) = \alpha_{01}\oint_{\gamma_h}\left(\dot{\theta}+\beta\theta\dot{\theta}+\gamma\theta^2\dot{\theta}\right)\,d\theta. \tag{3.15}$$

We write the Poincaré-Melnikov function using an integral quotient as follows

$$\begin{aligned} I(h,\eta) &= \alpha_{01}\left(I_0(h,\eta)+\beta I_1(h,\eta)+\gamma\, I_2(h,\eta)\right), &(3.16)\\ &= \alpha_{01}I_0(h,\eta)\left(1+\beta\, Q_{10}(h,\eta)+\gamma\, Q_{20}(h,\eta)\right), &(3.17)\end{aligned}$$

where $Q_{10}(h,\eta) = \frac{I_1(h,\eta)}{I_0(h,\eta)}$, $Q_{20}(h,\eta) = \frac{I_2(h,\eta)}{I_0(h,\eta)}$, $I_0(h,\eta) = \int_{\theta_0(h)}^{\theta_1(h)}\dot{\theta}d\theta$, $I_1(h,\eta) = \int_{\theta_0(h)}^{\theta_1(h)}\theta\dot{\theta}d\theta$, $I_2(h,\eta) = \int_{\theta_0(h)}^{\theta_1(h)}\theta^2\dot{\theta}d\theta$, $\dot{\theta} = \sqrt{G(\theta,\eta)}$ with $G(\theta,\eta) = 2h-\theta^2+\frac{2}{3}\theta^3-\frac{\eta}{2}\theta^4$, and the boundaries of the integrals, $\theta_0(h)$ and $\theta_1(h)$, are the negative and the positive root of $G(\theta,\eta)$ closest to the center point, respectively. We have calculated $Q_{10}(h,\eta)$ and $Q_{20}(h,\eta)$ for several values of η, numerically. These numerical results indicate that $\frac{dQ_{10}}{dh}(h,\eta) > 0$ and $\frac{dQ_{20}}{dh}(h,\eta) > 0$, see Figure 5. So, based on these numerical results we conjecture the monotonicity of $Q_{10}(h,\eta)$ and $Q_{20}(h,\eta)$. Following from the signs of parameters β and γ (both negative), we see that equation (3.17) has at most one zero. This means that the system has at most one limit cycle. This limit cycle exists if and only if $I(h_{\,max},\eta) < 0$. If $h = h_0$ is a zero of $I(h,\eta)$, we get $\frac{dI}{dh}(h_0,\eta) = 2\alpha_{01}I_0(h_0,\eta)\left(\beta\,\frac{dQ_{10}}{dh}(h_0,\eta)+\gamma\,\frac{dQ_{20}}{dh}(h_0,\eta)\right) < 0$. So we

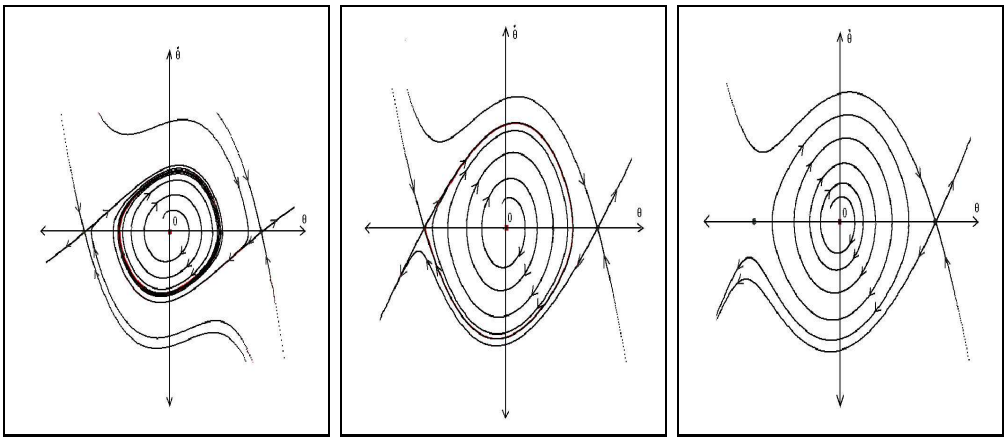

(a) $\kappa = 0.1$ (b) $\kappa = 0.317$ (c) $\kappa = 0.4$

Figure 6: Phase portraits of cubic nonsymmetrical $C_N(\alpha)$ case for $c_1 = -3$, $c_2 = 0.25$, $c_3 = 1$, and $\tilde{\epsilon} = 0.08$.

conclude that the limit cycle is always stable.
Numerical results for some special values of the parameters are given in Figure 6. For $\kappa = 0.1$ we see the stable limit cycle. For $\kappa = 0.317$ the limit cycle disappears in a homoclinic bifurcation. For $\kappa = 0.4$ the system is globally unstable and any initial disturbance leads to an unbounded solution.

4 Analysis of the model equation for nonlinear structural stiffness

In this section, we consider the existence, the stability, and the bifurcation of limit cycles for the single seesaw oscillator with nonlinear stiffness forces, given by equation (2.8). We rescale equation (2.8) with the transformation $\theta \rightarrow c\,\bar{\theta}$, then, after neglecting the "bar" and choosing $c = \frac{-1}{\alpha_{20}}$ with $\alpha_{20} \neq 0$, we get

$$\ddot{\theta} + \theta - \theta^2 + \eta\theta^3 = \tilde{\epsilon}\alpha_{01}\left(\dot{\theta} + \beta\theta\dot{\theta} + \gamma\theta^2\dot{\theta}\right) + \mathcal{O}(\tilde{\epsilon}^2), \tag{4.1}$$

where $\eta = \frac{\alpha_{30}}{\alpha_{20}^2} < 0$, $\beta = \frac{-\alpha_{11}}{\alpha_{01}\,\alpha_{20}}$ and $\gamma = \frac{\alpha_{21}}{\alpha_{01}\alpha_{20}^2} < 0$.
This is a perturbed Hamiltonian system with Hamiltonian

$$H(\theta, \dot{\theta}, \eta) = \frac{1}{2}\dot{\theta}^2 + \frac{1}{2}\theta^2 - \frac{1}{3}\theta^3 + \frac{\eta}{4}\theta^4. \tag{4.2}$$

Note that this equation is the same equation as found for the oscillator with linear stiffness for the cubic nonsymmetrical case, equation (3.12). The only difference is that the sign of the parameter β may now be positive.
We consider the existence of bifurcations that create or destroy periodic solutions. First

we study the existence of homoclinic bifurcations depending on the parameters η, β, and γ. Recall that a homoclinic bifurcation occurs if the Poincaré-Melnikov function $I(h,\eta)$ is zero for $h = h_{max}$. Using equation (3.16) we get the equation

$$I_0(h_{max},\eta) + \beta I_1(h_{max},\eta) + \gamma I_2(h_{max},\eta) = 0. \tag{4.3}$$

If we set γ as a function of the parameters η and β then we obtain

$$\gamma(\eta,\beta) = -\frac{I_1(h_{max},\eta)}{I_2(h_{max},\eta)}\beta - \frac{I_0(h_{max},\eta)}{I_2(h_{max},\eta)}, \tag{4.4}$$

where both of $\frac{I_1(h_{max},\eta)}{I_2(h_{max},\eta)}$ and $\frac{I_0(h_{max},\eta)}{I_2(h_{max},\eta)}$ are positive.
For a fixed value of η, say η_0, we obtain a line in the (β,γ)-parameter plane on which the homoclinic bifurcation occurs, see Figure 7:

$$\gamma(\eta_0,\beta) = -\frac{I_1(h_{max},\eta_0)}{I_2(h_{max},\eta_0)}\beta - \frac{I_0(h_{max},\eta_0)}{I_2(h_{max},\eta_0)}. \tag{4.5}$$

Another type of bifurcation may occur if the Poincaré-Melnikov function has multiple roots. In particular, a saddle-node bifurcation of periodic solutions appears if both $I(h,\eta)$ and $\frac{\partial I}{\partial h}(h,\eta)$ are zero and $\frac{\partial^2 I}{\partial h^2}(h,\eta) \neq 0$ for some $(h,\eta) = (h_0,\eta_0)$, i.e. if

$$\begin{aligned} I_0(h,\eta) + \beta I_1(h,\eta) + \gamma I_2(h,\eta) &= 0, & (4.6)\\ \frac{\partial I_0}{\partial h}(h,\eta) + \beta\frac{\partial I_1}{\partial h}(h,\eta) + \gamma\frac{\partial I_2}{\partial h}(h,\eta) &= 0, & (4.7) \end{aligned}$$

for some $(h,\eta) = (h_0,\eta_0)$. Solving equation (4.6, 4.7) for β and γ for a fixed value of η, say η_0, we obtain a curve in the (β,γ)-parameter plane on which the saddle node bifurcation occurs (write $J_i = \frac{\partial I_i}{\partial h}$),

$$\begin{pmatrix}\beta(h,\eta_0)\\ \gamma(h,\eta_0)\end{pmatrix} = \frac{-1}{I_1(h,\eta_0)J_2(h,\eta_0) - J_1(h,\eta_0)I_2(h,\eta_0)}\begin{pmatrix}J_2(h,\eta_0) & -I_2(h,\eta_0)\\ -J_1(h,\eta_0) & I_1(h,\eta_0)\end{pmatrix}\begin{pmatrix}I_0(h,\eta_0)\\ J_0(h,\eta_0)\end{pmatrix}. \tag{4.8}$$

This curve is parameterized by h. It terminates on the homoclinic bifurcation line at the point $(\beta_0,\gamma_0) = (\beta(h_{max},\eta_0),\gamma(h_{max},\eta_0))$. Note that (β_0,γ_0) may be viewed as an 'organizing center' in the parameter plane in the sense that all different dynamical behaviour can be found in a neighbourhood of this point. We obtain the bifurcation diagram as shown in Figure 7. The bifurcation curves divide the (β,γ)-parameter plane into three regions, that is,

- A_0 is the region where we have no limit cycle,
- A_1 is the region where we have only one limit cycle,
- A_2 is the region where we have two limit cycles.

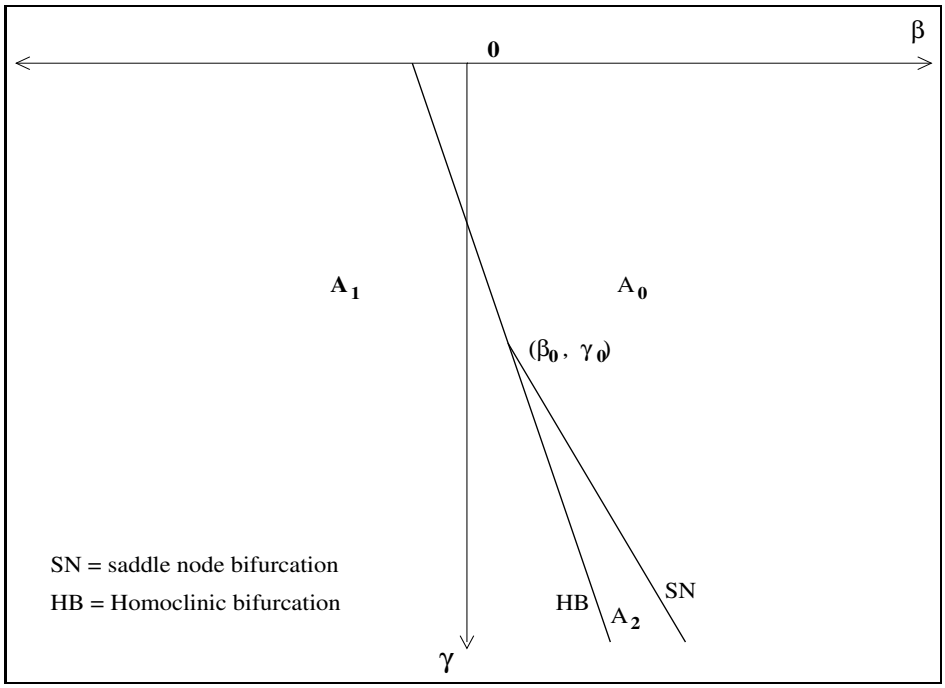

Figure 7: Bifurcation diagram in the (β, γ)-parameter plane.

The number of limit cycles in each region is determined from the number of roots of the Poincaré-Melnikov function in that region, as shown in Figure 8. For $\beta < 0$ we are back in the situation of section 3.3: below the homoclinic bifurcation line we have a stable limit cycle, above this line no limit cycle is found (see Figure 6 for some phase-portraits for this case).
For $\beta > 0$ the situation is quite different. Starting on the line $\gamma = 0$, we find readily that $I(h, \eta)$ is positive for $h \in (0, h_{max}]$ and no limit cycle is found. On decreasing γ from zero for positive but fixed β, the Poincaré-Melnikov function remains positive for $h \in (0, h_{max}]$ until either the homoclinic or saddle-node bifurcation curve is reached. In the region A_0 therefore no limit cycles are found.
If β is chosen such that on decreasing γ the homoclinic curve is reached first, then a homoclinic bifurcation occurs in which a stable limit cycle is born. The stability of this limit cycle, $\Gamma(h_0)$, follows from $\frac{\partial I}{\partial h}(h_0, \eta_0) < 0$. In the region A_1, therefore we have one stable limit cycle.
If β is chosen such that on decreasing γ the saddle node curve is reached first, two limit cycles are created in a saddle-node bifurcation. The smaller limit cycle being stable and the larger one being unstable. These limit cycles persist in the region A_2 where the Poincaré-Melnikov function has two zeroes. Finally, on reaching the homoclinic curve from region A_2, the unstable limit cycle disappears in a homoclinic bifurcation and we enter region A_1.
In the three dimensional (η, β, γ)-parameter space, equation (4.3) defines a surface on which the homoclinic bifurcations occur. Figure 9(a) shows for some fixed values of η the projection of the homoclinic bifurcation lines on the (β, γ)-bifurcation plane. We see that

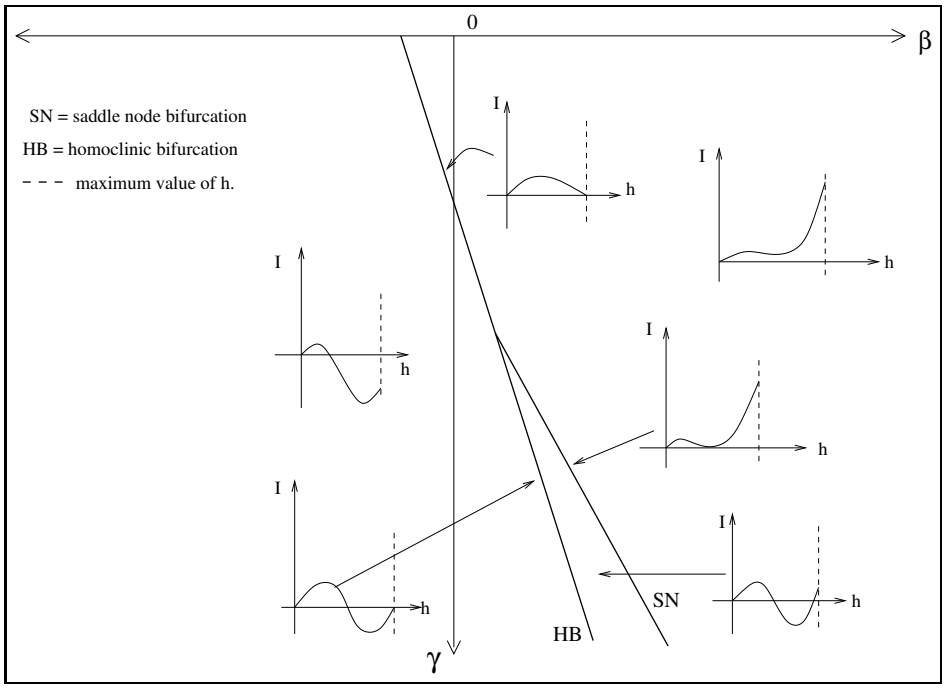

Figure 8: The various shapes of the Poincaré Melnikov functions in the (β, γ)-parameter plane.

if we increase the value of η then the homoclinic bifurcation line decreases. Figure 9(b) shows the surface of homoclinic bifurcation in three dimensions. We have one limit cycle for all (η, β, γ) below of that surface and there is a possibility to get either no limit cycle or two limit cycles above of that surface.
Similarly equations (4.6-4.7) define a surface on which the saddle-node bifurcations occur. The intersection of these surfaces defines a curve $(\beta_0(\eta), \gamma_0(\eta))$ consisting of all the points where the saddle-node bifurcation curves end on the homoclinic bifurcation lines. Figure 10(a) shows for some fixed values of η the projection of the saddle-node bifurcation curves in (β, γ)-plane. Also shown is the projection of the curve consisting of termination points.
Figure 10(b) shows the homoclinic and the saddle node bifurcations for $\eta = -6, \cdots, -1$ in (η, β, γ)-space. From equations (4.6-4.7) we have a termination curve as a set of the intersection points which are the solutions for both equations at $h = h_{max}$. Figure 11(a) shows the termination curve in (η, β, γ)-space.
Now we consider some numerical results for special values of the parameters β, η and γ. We choose $\beta = 400$, $\eta = -1$ and γ equal to respectively -430, -487, and -530. Effectively we move from region A_0, through A_2 to A_1, see Figure 12. For $\gamma = -430$ the system is globally unstable and any initial disturbance leads to an unbounded solution. For $\gamma = -487$ we have two limit cycles, the small limit cycle is stable and the big one is unstable. For $\gamma = -530$ we have only one stable limit cycle left. We consider finally the period of oscillation of the limit cycles. Suppose $I(h_0, \eta_0) = 0$, then the limit cycle is to

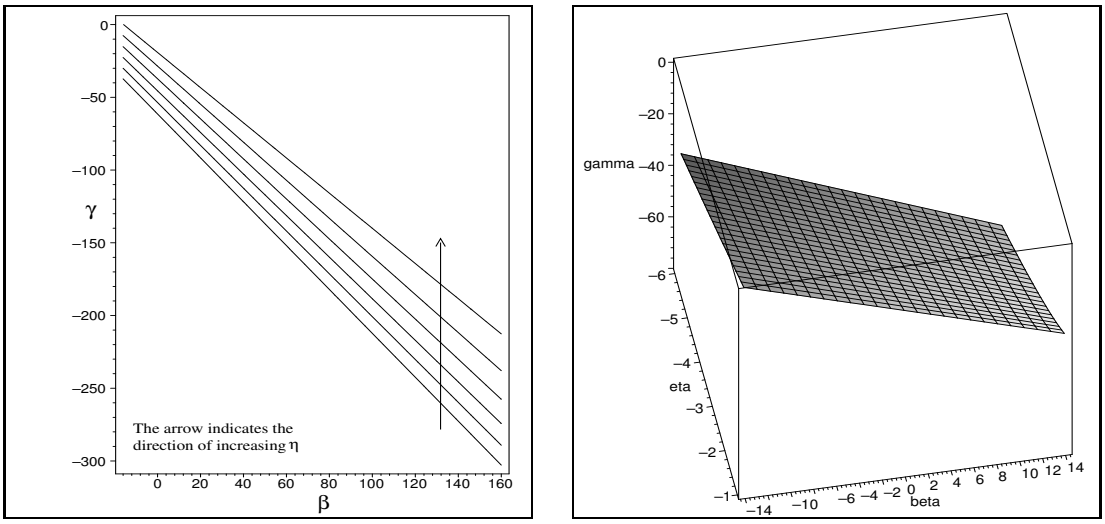

(a) 2-d homoclinic bifurcation (b) 3-d homoclinic bifurcation

Figure 9: Numerical results of homoclinic bifurcations.

$O(\epsilon)$ approximated by the unperturbed orbit $\Gamma(h_0, \eta_0)$. The period of the limit cycle is then approximated to $O(\epsilon)$ by the period $T_{\Gamma(h_0,\eta_0)}$ of $\Gamma(h_0, \eta_0)$, given by

$$T_{\Gamma(h_0,\eta_0)} = \int_{\Gamma(h_0,\eta_0)} \frac{d\theta}{\dot{\theta}} d\theta = \int_{\theta_0(h)}^{\theta_1(h)} \frac{2d\theta}{\sqrt{2h - \theta^2 + \frac{2}{3}\theta^3 - \frac{\eta}{2}\theta^4}} d\theta, \tag{4.9}$$

where the boundaries of the integral, $\theta_0(h_0)$ and $\theta_1(h_0)$, are the intersection points of $\Gamma(h_0, \eta_0)$ with the θ-axis. These points follow as the zeroes of $2h_0 - \theta^2 + \frac{2}{3}\theta - \frac{\eta_0}{2}\theta^4$, inside of the homoclinic loop. Assuming again $\beta = 400$ and $\eta = -1$ we consider the period of the limit cycles when γ is varied from -550 to -480, see Figure 11(b). Decreasing γ from -480 we first find the saddle-node bifurcation for $\gamma = \gamma_{sn} = -485.0156648$ in which the two limit cycles are born. The period of the (shrinking) stable limit cycle decreases when γ is further decreased. The period of the (expanding) unstable limit cycle increases when γ is further decreased. The period of the unstable limit cycle grows to infinity when it approaches the homoclinic loop $\Gamma(h_{max})$. Then, in the homoclinic bifurcation, occurring for $\gamma = \gamma_{hom} = -523.3769812$, the unstable limit cycle disappears.

5 Conclusions

We considered in this paper the aeroelastic response of a one degree-of-freedom structure of single seesaw oscillator under strong wind conditions. The model equation describing the aeroelastic oscillations is adapted from [7] and reads

$$\ddot{\theta} + \theta + p_2\theta^2 + p_3\theta^3 = \epsilon(-2\xi\dot{\theta} + u^2 C_N(\alpha)). \tag{5.10}$$

In this equation θ denotes the angle of rotation of the seesaw structure around the hinge axis. We assume $p_3 < 0, c_1 < 0$, and $c_3 \geq 0$. Assuming furthermore a strong wind

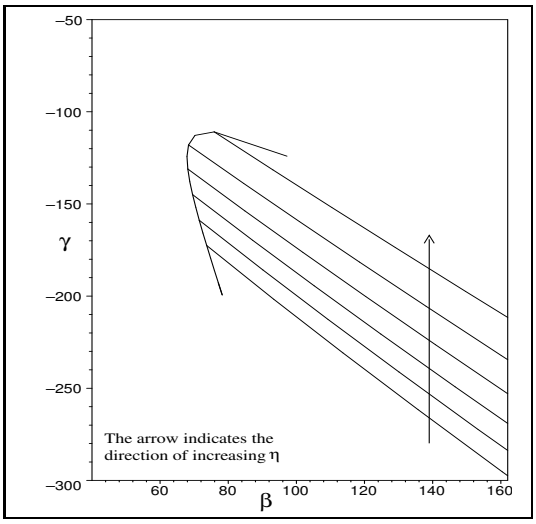

(a) 2-d saddle node bifurcation

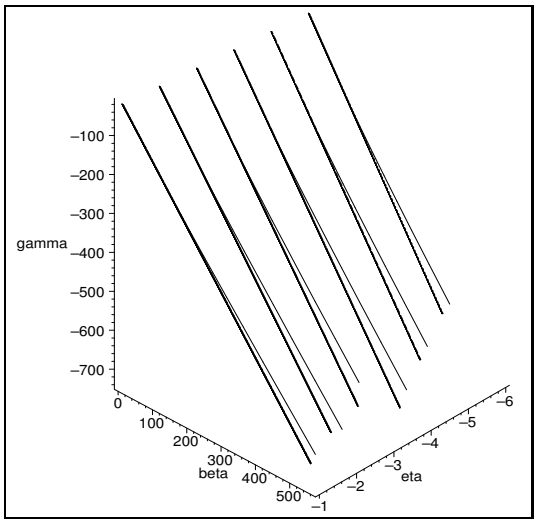

(b) 3-d homoclinic and saddle node bifurcations

Figure 10: Numerical results of homoclinic and saddle node bifurcations.

velocity u and introducing a new parameter $\kappa = \epsilon u^2 = \mathcal{O}(1)$ and a new small parameter $\tilde{\epsilon} = \epsilon u = \sqrt{\epsilon\kappa}$ to equation (5.10), we get a strongly nonlinear system as follows

$$\ddot{\theta} + \theta + \alpha_{20}\theta^2 + \alpha_{30}\theta^3 = \tilde{\epsilon}\,\left(\alpha_{01}\,\dot{\theta} + \alpha_{11}\theta\,\dot{\theta} + \alpha_{21}\theta^2\dot{\theta}\right) + \mathcal{O}(\tilde{\epsilon}^2), \tag{5.11}$$

where α_{20} and α_{30} contain both structural and aerodynamic stiffness forces. We consider first the oscillator with linear structural stiffness, i.e. equation (5.11) with $p_2 = p_3 = 0$, for three choices of the aerodynamic parameters.

1. Case $c_2 = 0$.
   Now the equation reads

   $$\ddot{\theta} + \theta + \tilde{\alpha}_{30}\theta^3 = \tilde{\epsilon}\,\left(\alpha_{01}\,\dot{\theta} + \alpha_{21}\theta^2\dot{\theta}\right) + \mathcal{O}(\tilde{\epsilon}^2). \tag{5.12}$$

   It is found that a stable limit cycle exists if and only if $\kappa < \frac{3}{-2c_1}$. For $\kappa = \frac{3}{-2c_1}$ a heteroclinic bifurcation destroys the limit cycle, and for $\kappa > \frac{3}{-2c_1}$ the system is globally unstable. That is, any initial disturbance leads to unbounded solutions.

2. Case $c_3 = 0$.
   Now the equation reads

   $$\ddot{\theta} + \theta + \tilde{\alpha}_{20}\theta^2 = \tilde{\epsilon}(\alpha_{01}\dot{\theta} + \alpha_{11}\theta\,\dot{\theta}) + \mathcal{O}(\tilde{\epsilon}^2). \tag{5.13}$$

   A stable limit cycle exists if and only if $\kappa < \frac{2}{-5c_1}$. For $\kappa = \frac{2}{-5c_1}$ a homoclinic bifurcation destroys the limit cycle, and for $\kappa > \frac{2}{-5c_1}$ the system is globally unstable.

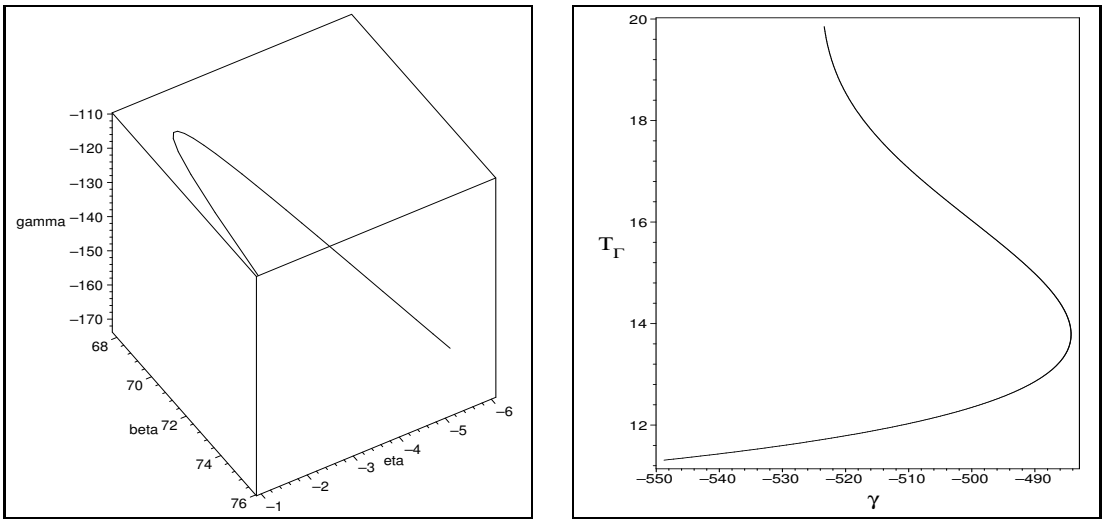

(a) Termination curve

(b) Period of limit cycles for $\eta = -1$, $\beta = 400$

Figure 11: Termination curve and period of limit cycles.

3. Case $c_2 \neq 0, c_3 \neq 0$.
   Now the equation reads

$$\ddot{\theta} + \theta - \theta^2 + \eta\,\theta^3 = \tilde{\epsilon}\,\alpha_{01}\left(\dot{\theta} + \beta\,\theta\,\dot{\theta} + \gamma\,\theta^2\dot{\theta}\right) + \mathcal{O}(\tilde{\epsilon}^2), \tag{5.14}$$

   where all of the parameters β, η, and γ are negative.
   Based on the numerical analysis we find at most one limit cycle, which, if it exists, is stable.

Secondly, we have considered the single seesaw oscillator with nonlinear structural stiffness. We obtain again equation (5.14) but now β may be positive. We find that, different from the previous cases, two limit cycles may co-exist. These two limit cycles are shown to be born in a saddle node bifurcation of periodic solutions. The smaller limit cycle is stable and the larger one is unstable. We have obtained regions in the (β, γ)-parameter plane where zero, one or two limit cycles are found. On the curves separating these regions we find homoclinic bifurcations or the mentioned saddle-node bifurcations. In the region with no limit cycle the system is globally unstable and any initial disturbance leads to unbounded solutions. Finally, we have considered the period of oscillation of the two co-existing limit cycles for a special case.

Acknowledgement
The author would like to thank Dr. T. I. Haaker and Dr. A. H. P. van der Burgh for the careful reading of the manuscript and several valuable comments and suggestions. This research project was sponsored by the Secondary Teacher Development Project (PGSM) - Indonesia with contract No. 6519/0300/Kont-Fel/PGSM and the University of Technology in Delft - The Netherlands.

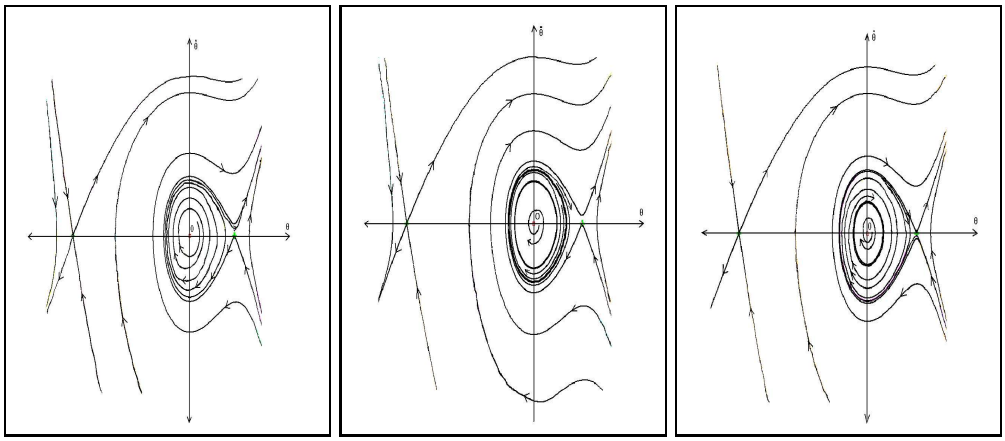

(a) $\gamma = -430$ (b) $\gamma = -487$ (c) $\gamma = -530$

Figure 12: Phase portraits for $\beta = 400$ and $\eta = -1$.

References

[1] R. D. Blevins, *Flow-Induced Vibration* 2^{nd} *Editon*, Van Nostrand Reinhold, New York, 1990.

[2] T.I. Haaker and A.H.P. van der Burgh, *On the dynamics of aeroelastic oscillators with one degree of freedom*, SIAM J, Appl. Math., Vol.54, No. 4, 1994, pp. 1033-1047.

[3] T. I. Haaker and B. W. van Oudheusden, *One-degree-of-freedom rotational galloping under strong wind conditions*, International journal of Non-linear Mechanics, Vol.32, no.5, 1997, pp. 803 - 814.

[4] A. Doelman and F. Verhulst, *Bifurcations of strongly non-linear self-excited oscillations*, Mathematical Methods in the applied sciences, Vol. 17, 1994 , pp. 189-207.

[5] W.T. van Horssen and R.E. Kooij, *Bifurcation of limit cycles in a particular class of quadratic systems with two centres*, Journal of differential equations, Vol. 114, No. 2, 1994, pp. 538-569.

[6] I.D. Iliev and L.M. Perko, *Higher order bifurcations of limit cycles*, Journal of differential equations, Vol. 154, 1999, pp. 339-363.

[7] T.I.Haaker, *Quasi-steady modelling and asymptotic analysis of aeroelastic oscillators*, Ph.D. Thesis, Department of Applied Analysis, University of Technology, Delft, 1996.

[8] A.A. Andronov, E.A. Leontovich, I.I. Gordon and A.G. Maier, *Theory of bifurcations of dynamical systems on plane, Israel program of scientific translations, Jerusalem*,Wiley, New York, 1973.

[9] T.R.Blows and L.M.Perko, *Bifurcation of limit cycles from centers and separatrix cycles of planar analytic system*, SIAM Review, vol.36., No.3., September 1994, pp 341-376.

[10] V. Prasolov and Y. Solovyev, *Elliptic Functions and Elliptic Integrals*, Translations of Mathematical Monographs vulome 170, American Mathematical Society, USA, 1997.

A Appendix 1 : Proof of the monotonicity of Q_{20}

In this appendix we consider the monotonicity proofs of integral quotients $Q_{10}(h)$ and $Q_{20}(h)$ of subsection 3.1 and subsection 3.2, respectively.
Firstly, we consider the monotonicity of $Q_{20}(h)$. From subsection 3.1 we get that $I_0(h) = \int_0^{\theta(h)} R(\theta)d\theta$, $I_2(h) = \int_0^{\theta(h)} \theta^2 R(\theta)d\theta$, and $Q_{20}(h) = \frac{I_2(h)}{I_0(h)}$ with $R(\theta) = \dot{\theta} = \sqrt{2h - \theta^2 + \frac{1}{2}\theta^4}$ and the upper boundary of the integrals, $\theta(h)$, is the smallest positive root of $R(\theta)$. Integrating by parts in $I_0(h)$ we obtain

$$I_0(h) = \int_0^{\theta(h)} \frac{\theta^2 - \theta^4}{R(\theta)} d\theta. \tag{A1-1}$$

Also

$$I_0(h) = \int_0^{\theta(h)} \frac{2h - \theta^2 + \frac{1}{2}\theta^4}{R(\theta)} d\theta. \tag{A1-2}$$

Similarly, we get

$$3I_2(h) = \int_0^{\theta(h)} \frac{\theta^4 - \theta^6}{R(\theta)} d\theta, \tag{A1-3}$$

and also

$$I_2(h) = \int_0^{\theta(h)} \frac{2h\theta^2 - \theta^4 + \frac{1}{2}\theta^6}{R(\theta)} d\theta. \tag{A1-4}$$

We write $I_i(h) = \int_0^{\theta(h)} \theta^i R(\theta)d\theta$ and $J_i(h) = \frac{dI_i}{dh}(h) = \int_0^{\theta(h)} \frac{\theta^i}{R(\theta)} d\theta, \quad i = 0, \cdots, 6.$
For simplification of writing, we write I_i, J_i, and Q_{20} instead of $I_i(h), J_i(h)$, and $Q_{20}(h)$, respectively. From their definition it follows that I_0, I_2, J_2, and J_4 are positive for $h > 0$. Also, since $\theta(h) \leq 1$, we know that $J_0 > J_2$.
Using the equations (A1-1 - A1-4) we can express I_0 and I_2 in terms of J_i as follows

$$\begin{aligned} I_0 &= J_2 - J_4, && \text{(A1-5)} \\ I_0 &= 2hJ_0 - J_2 + \frac{1}{2}J_4, && \text{(A1-6)} \\ 3I_2 &= J_4 - J_6, && \text{(A1-7)} \\ I_2 &= 2hJ_2 - J_4 + \frac{1}{2}J_6. && \text{(A1-8)} \end{aligned}$$

Combining equations (A1-5 - A1-6) we get $J_4 = \frac{4}{3}(J_2 - hJ_0)$. Using the equations (A1-5 - A1-8) we obtain

$$\begin{aligned} 15I_0 &= 20hJ_0 - 5J_2, && \text{(A1-9)} \\ 15I_2 &= 12hJ_2 - 3J_4. && \text{(A1-10)} \end{aligned}$$

Because of $J_4 > 0$ we find $(J_2 - hJ_0) > 0$ and from equation (A1-10) we obtain $(4hJ_0 - J_2) > 0$. A straightforward calculation yields

$$\begin{aligned} 15(J_2I_0 - J_0I_2) &= J_2(20hJ_0 - 5J_2) - J_0(12hJ_2 - 3J_4), \\ &= J_2(4hJ_0 - J_2) + 4(J_0 - J_2)(J_2 - hJ_0), \\ &> 0. && \text{(A1-11)} \end{aligned}$$

Consider again the derivative of the integral quotient, i.e.

$$\frac{dQ_{20}}{dh} = \frac{J_2 I_0 - J_0 I_2}{I_0^2}. \tag{A1-12}$$

Then from the inequality (A1-11) we obtain immediately that $\frac{dQ_{20}}{dh} > 0$. This implies that the integral quotient Q_{20} is a strictly increasing function in h.

B Appendix 2 : Proof of the monotonicity of Q_{10}

We now consider the monotonicity of $Q_{10}(h)$. From subsection 3.2 we get that $I_0(h) = \int_{\theta_0(h)}^{\theta_1(h)} R(\theta)d\theta$, $I_1(h) = \int_{\theta_0(h)}^{\theta_1(h)} \theta R(\theta)d\theta$, and $Q_{10}(h) = \frac{I_1(h)}{I_0(h)}$ with $R(\theta) = \dot{\theta} = \sqrt{2h - \theta^2 + \frac{2}{3}\theta^3}$ and the boundaries of the integrals, $\theta_0(h)$ and $\theta_1(h)$, are the negative root and the smallest positive root of $R(\theta)$, respectively. Integrating by parts in $I_0(h)$ we obtain

$$I_0(h) = \int_{\theta_0(h)}^{\theta_1(h)} \frac{\theta^2 - \theta^3}{R(\theta)} d\theta. \tag{A2-1}$$

Also

$$I_0(h) = \int_{\theta_0(h)}^{\theta_1(h)} \frac{2h - \theta^2 + \frac{2}{3}\theta^3}{R(\theta)} d\theta. \tag{A2-2}$$

Similarly, we get

$$2I_1(h) = \int_{\theta_0(h)}^{\theta_1(h)} \frac{\theta^3 - \theta^4}{R(\theta)} d\theta, \tag{A2-3}$$

and also

$$I_2(h) = \int_{\theta_0(h)}^{\theta_(h)} \frac{2h\theta - \theta^3 + \frac{2}{3}\theta^4}{R(\theta)} d\theta. \tag{A2-4}$$

We again write $I_i(h) = \int_{\theta_0(h)}^{\theta_1(h)} \theta^i R(\theta)d\theta$ and $J_i(h) = \frac{dI_i}{dh}(h) = \int_{\theta_0(h)}^{\theta_1(h)} \frac{\theta^i}{R(\theta)} d\theta, \quad i = 0, \cdots, 4.$
Using the equations (A2-1 - A2-4) we can express I_0 and I_2 in terms of J_i, as follows

$$\begin{aligned} I_0 &= J_2 - J_3, && \text{(A2-5)} \\ I_0 &= 2hJ_0 - J_2 + \frac{2}{3}J_3, && \text{(A2-6)} \\ 2I_1 &= J_3 - J_4, && \text{(A2-7)} \\ I_1 &= 2hJ_1 - J_3 + \frac{2}{3}J_4. && \text{(A2-8)} \end{aligned}$$

Combining equations (A2-5 - A2-6) we obtain $J_3 = \frac{6}{5}(J_2 - hJ_0)$. Also, applying a theorem of Legendre [10], we get $J_1 = J_2$. Using the equations (A2-5 - A2-8) we obtain

$$\begin{aligned} 5I_0 &= 6hJ_0 - J_1, && \text{(A2-9)} \\ 7I_1 &= 6hJ_1 - J_3. && \text{(A2-10)} \end{aligned}$$

It follows from their definition that I_0, I_1, and J_i are positive for $h > 0$. Also, since $\theta_0(h) < 0$ and $\theta_1(h) > 0$, we know that $J_0 - J_1 > 0$. As $J_3 > 0$ also $J_1 - hJ_0 > 0$. Finally, from equation (A2-9) we get $6hJ_0 - J_1 > 0$.
A straightforward calculation now yields

$$\begin{aligned} 35(J_1I_0 - J_0I_1) &= J_1(42hJ_0 - 7J_1) + J_0(6(5h-1)J_1 + 6hJ_0), \\ &= (12hJ_0J_1 - 7J_1^2) + (6J_0J_1 - 6hJ_0^2), \\ &= (6hJ_0 - J_1)J_1 + 6(J_0 - J_1)(J_1 - hJ_0), \\ &> 0. && \text{(A2-11)} \end{aligned}$$

Consider again the derivative of the integral quotient, i.e.

$$\frac{dQ_{10}}{dh} = \frac{J_1 I_0 - J_0 I_1}{I_0^2}. \tag{A2-12}$$

Then from the inequality (A2-11) we obtain immediately that $\frac{dQ_{10}}{dh} > 0$. This implies that the integral quotient Q_{10} is a strictly increasing function in h.